Higher Order Responses of Three-Dimensional Elastic Plate-Like Structures and their Visualization

Monique Dauge[&], Andreas Rössle[*] and Zohar Yosibash[#]

[&] Institut Mathématique, UMR 6625 du CNRS, Université de Rennes 1, Campus de Beaulieu, 35042 Rennes, France

[*] Mathematisches Institut A, Universität Stuttgart, Pfaffenwaldring 57 70569 Stuttgart, Germany

[#] Pearlstone Center for Aeronautical Engineering Studies, Mechanical Engineering Dept., Ben-Gurion University of the Negev, Beer-Sheva, Israel

Abstract. *The displacement of three-dimensional linearly elastic plate-like domains can be expanded as a compound power series asymptotics, when the thickness parameter ε tends to zero. The leading term $\boldsymbol{u}^0$ in this expansion is the well-known Kirchhoff-Love displacement field, which is the solution to the limit case when $\varepsilon \to 0$. Herein we focus our discussion on plate-like domains with either clamped or free lateral boundary conditions, and characterize the loading conditions for which the leading term vanishes. In these situations the first non-zero term $\boldsymbol{u}^k$ in the expansion appears for $k = 2$, 3 or 4 and is denoted as higher-order response of order 2, 3 or 4 respectively. The mathematical analysis for higher-order responses is backed-up by numerical simulation using the p-version finite element method.*

1 INTRODUCTION

Plate-like domains are three-dimensional structures with one of their dimensions, usually denoted by "thickness" (2ε), much smaller compared to the other two dimensions. In the linear theory of elasticity, the displacements solution $\boldsymbol{u}$ is of interest and can be considered as a function of the coordinates $\boldsymbol{x}$ and of ε: $\boldsymbol{u} = \boldsymbol{u}(\boldsymbol{x}, \varepsilon)$. If the loadings behave uniformly with respect to ε, see (2.2)-(2.3) later, it is natural to expand $\boldsymbol{u}(\boldsymbol{x}, \varepsilon)$ as an asymptotic series in ε. It is now well understood that this problem has a singular perturbation nature as $\varepsilon \to 0$ giving rise to boundary layer effects, and that such an expansion can be provided in the general form, compare with [8, 9, 11],

$$\boldsymbol{u}(\boldsymbol{x}, \varepsilon) \simeq \boldsymbol{u}^0(\boldsymbol{x}, \frac{\boldsymbol{x}}{\varepsilon}) + \varepsilon\, \boldsymbol{u}^1(\boldsymbol{x}, \frac{\boldsymbol{x}}{\varepsilon}) + \varepsilon^2 \boldsymbol{u}^2(\boldsymbol{x}, \frac{\boldsymbol{x}}{\varepsilon}) + \cdots + \varepsilon^k \boldsymbol{u}^k(\boldsymbol{x}, \frac{\boldsymbol{x}}{\varepsilon}) \cdots \tag{1.1}$$

Detailed mathematical analysis on the asymptotics in thin isotropic plates, see [10, 4, 5] for clamped plates and [6] for other lateral boundary conditions, makes it possible to explicitly quantify the various terms in the expansion (1.1). Moreover, numerical realization of several terms in (1.1) has been presented in [7].

Herein we address plates with either *hard-clamped* or *free* lateral boundary conditions, and based on the mathematical analysis in [3, 2] describe the loading conditions for which the leading term $\boldsymbol{u}^0$ vanishes in the expansion (1.1), providing a displacement field with a first non-vanishing term which is not $\boldsymbol{u}^1$ (that is zero too) but $\boldsymbol{u}^2$ (or even $\boldsymbol{u}^3$ or $\boldsymbol{u}^4$) denoted as higher-order response of order 2 (resp. 3 or 4). In these situations it may happen that a boundary layer term of the *same* order as the actual leading term appears in the displacement field. In the same spirit than [7], we visualize these higher-order responses using the p-version of the finite element method.

This paper is organized as follows: In Section 2 we provide the necessary notations and preliminaries followed by explicit details on the three-dimensional solution for clamped and free plates. In Section 3 the necessary conditions on the loadings to provide higher-order responses are summarized, followed by numerical visualization of the mathematical analysis in Section 4. These numerical solutions are obtained using the p-version finite element method. We conclude in Section 5.

2 NOTATIONS AND PRELIMINARIES

2.1 The elasticity problem

We consider a thin elastic, isotropic and homogeneous three-dimensional domain Ω defined as follows:

$$\Omega = \omega \times (-\varepsilon, +\varepsilon), \quad \text{with } \omega \subset \mathbb{R}^2 \text{ a regular domain,}$$

and associated cartesian coordinates are $\boldsymbol{x} = (x_1, x_2, x_3)$, see Figure 1.

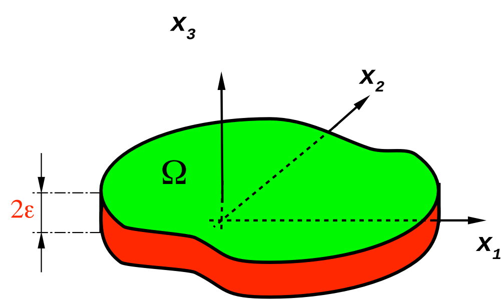

Figure 1: *Typical plate of interest and notations.*

Let $(u_1,\ u_2,\ u_3)^T$ denote the components of the displacement and let $\boldsymbol{e}$ denote the linearized strain tensor $e_{ij} = \frac{1}{2}(\partial_i u_j + \partial_j u_i)$, where $\partial_i \equiv \partial/\partial x_i$. The stress tensor $\boldsymbol{\sigma}$ is given by Hooke's law $\boldsymbol{\sigma} = [A]\,\boldsymbol{e}$, where $[A] = (A_{ijkl})$ is the compliance tensor of an isotropic material expressed in terms of the Lamé constants λ and μ:

$$A_{ijkl} = \lambda\,\delta_{ij}\delta_{kl} + \mu(\delta_{ik}\delta_{jl} + \delta_{il}\delta_{jk}).$$

In the sequel we will use either the Lamé constants or the equivalent engineering material coefficients:

$$\text{Young modulus} \quad E = \frac{\mu(3\lambda + 2\mu)}{\lambda + \mu} \quad \text{and Poisson ratio} \quad \nu = \frac{\lambda}{2(\lambda + \mu)} \,.$$

The tractions (surface forces) are denoted by $\boldsymbol{t} = \boldsymbol{\sigma} \cdot \boldsymbol{n}$, where $\boldsymbol{n}$ is the outward normal vector on the domain's boundary. We consider herein either clamped ($\boldsymbol{u} = \boldsymbol{0}$), or free ($\boldsymbol{t} = \boldsymbol{0}$) boundary conditions on the lateral face of the plate:

$$\partial\Omega_L = \partial\omega \times (-\varepsilon, +\varepsilon) \,.$$

The tractions on the upper face of the plate ($\Gamma^+ = \{\boldsymbol{x} \,|\, x_3 = \varepsilon\}$) and the corresponding lower face of the plate ($\Gamma^- = \{\boldsymbol{x} \mid x_3 = -\varepsilon\}$) are denoted by $\boldsymbol{t}^+$ (corr. $\boldsymbol{t}^-$). The volume forces are denoted by $\boldsymbol{f}$.

With above notation, we may state the weak formulation of the elasticity problem for the free plate:

$$\begin{cases} \textbf{Seek} \quad \boldsymbol{u} \in H^1(\Omega)^3, \ \text{such that} \\ \displaystyle\int_\Omega [A]\, \boldsymbol{e}(\boldsymbol{u}) : \boldsymbol{e}(\boldsymbol{v}) = \int_\Omega \boldsymbol{f} \cdot \boldsymbol{v} + \int_{\Gamma^+} \boldsymbol{t}^+ \cdot \boldsymbol{v} + \int_{\Gamma^-} \boldsymbol{t}^- \cdot \boldsymbol{v} \,, \quad \forall \boldsymbol{v} \in H^1(\Omega)^3 \end{cases} \tag{2.1}$$

whereas for the clamped plate one simply needs to seek a solution in the space $[H^1_{\partial\Omega_L}]^3$, which are functions in $H^1(\Omega)^3$ with the additional constraint that $\boldsymbol{u} = \boldsymbol{0}$ on $\partial\Omega_L$.

Of course, in the case of free boundary conditions the applied tractions $\boldsymbol{t}^\pm$ and the volume forces $\boldsymbol{f}$ are supposed to be equilibrated versus the rigid displacements.

2.2 Scaled coordinates and assumptions on data

We denote by the Greek index α the in-plane variables $\{1, 2\}$, by s a curvilinear coordinate along $\partial\omega$ and by n the distance to $\partial\omega$. We also use the subscripts $_n$ and $_s$ for the normal and tangential components of a field on the boundary $\partial\omega$.

The subscript $_*$ is used as condensed notation of in-plane variables. Thus we denote: $\boldsymbol{x}_* \stackrel{\text{def}}{=} (x_1, x_2)$, $\boldsymbol{u}_* \stackrel{\text{def}}{=} (u_1, u_2)^T$, $\operatorname{div}_* \boldsymbol{u}_* \stackrel{\text{def}}{=} \partial_1 u_1 + \partial_2 u_2$, $\nabla_* = (\partial_1, \partial_2)^T$ and $\Delta_* \stackrel{\text{def}}{=} \partial_{11} + \partial_{22}$

It is convenient to represent all quantities of an asymptotic expansion in a fixed reference domain, thus we stretch the plate along the vertical axis and define the stretched transverse variable

$$X_3 \stackrel{\text{def}}{=} x_3/\varepsilon.$$

Moreover, a correct description of the boundary layer terms requires the introduction of the stretched distance to $\partial\omega$:

$$N \stackrel{\text{def}}{=} n/\varepsilon.$$

In such an asymptotic analysis, it is natural to assume that the volume forces behave as fixed profiles in the scaled vertical variable X_3 , compare with the reference work [1].

Moreover, like in the previous works [3, 2, 6], we suppose that they are of order of ε in the vertical direction, and of order $\mathcal{O}(1)$ in the in-plane directions, namely

$$f_\alpha(\boldsymbol{x}) = F_\alpha(x_1, x_2, X_3), \qquad f_3(\boldsymbol{x}) = \varepsilon F_3(x_1, x_2, X_3) \tag{2.2}$$

with the data $\boldsymbol{F} = (F_1, F_2, F_3)^T$ regular up to the boundary, i.e. $\boldsymbol{F} \in C^\infty(\overline{\omega} \times [-1\,,\,1])^3$. Correspondingly we assume for the tractions on the upper and lower faces of the plate:

$$t_\alpha^\pm(\boldsymbol{x}) = \varepsilon T_\alpha^\pm(x_1, x_2, X_3 = \pm\varepsilon), \qquad t_3(\boldsymbol{x}) = \varepsilon^2 T_3^\pm(x_1, x_2, X_3 = \pm\varepsilon). \tag{2.3}$$

The above assumptions are the correct ones so that the *scaled* displacement $\widetilde{u}(x_1, x_2, X_3)$ defined as $(\boldsymbol{u}_*, \varepsilon u_3)(\boldsymbol{x})$ has a limit (which is generically non-zero) as $\varepsilon \to 0$.

Note that, as we are in the framework of linearized elasticity, by superposition we can construct displacement asymptotics for any volume forces $\boldsymbol{f}(\boldsymbol{x}, \varepsilon)$ and tractions $\boldsymbol{t}^\pm(\boldsymbol{x}, \varepsilon)$ which can be expanded as power series of ε.

2.3 The three-dimensional solution

Due to the symmetry properties of isotropic plates, it is well known that the displacements $\boldsymbol{u}$ can be split into a bending part and a membrane (or stretching) part according to

$$\begin{aligned}
\boldsymbol{u}_{\mathrm{b},\alpha}(x_3) &= \tfrac{1}{2}\big(\boldsymbol{u}_\alpha(x_3) - \boldsymbol{u}_\alpha(-x_3)\big), \qquad & \boldsymbol{u}_{\mathrm{b},3}(x_3) &= \tfrac{1}{2}\big(\boldsymbol{u}_3(x_3) + \boldsymbol{u}_3(-x_3)\big)\\
\boldsymbol{u}_{\mathrm{m},\alpha}(x_3) &= \tfrac{1}{2}\big(\boldsymbol{u}_\alpha(x_3) + \boldsymbol{u}_\alpha(-x_3)\big), \qquad & \boldsymbol{u}_{\mathrm{m},3}(x_3) &= \tfrac{1}{2}\big(\boldsymbol{u}_3(x_3) - \boldsymbol{u}_3(-x_3)\big).
\end{aligned}$$

$\boldsymbol{u}_\mathrm{b}$ is the solution of (2.1) corresponding to the bending parts of the volume forces $\boldsymbol{f}_\mathrm{b}$ and tractions $\boldsymbol{t}_\mathrm{b}$, and similarly for the membrane.

We are going to describe now, based on [6] (see also the presentation in [7]), the asymptotic expansion of $\boldsymbol{u}(\boldsymbol{x}, \varepsilon)$ under the assumptions (2.2)-(2.3). This expansion involves three sorts of terms:

i) Kirchhoff-Love displacements,

ii) Displacements $\boldsymbol{v} = \boldsymbol{v}(\boldsymbol{x}_*, X_3)$ with zero integral mean value

$$\forall\, \boldsymbol{x}_* \in \overline{\omega} \qquad \int_{-1}^{+1} \boldsymbol{v}(\boldsymbol{x}_*, X_3)\, dX_3 = 0\,,$$

iii) Boundary layer terms $\boldsymbol{\varphi} = \boldsymbol{\varphi}(s, N, X_3)$ exponentially decreasing as $N \to \infty$.

The Kirchhoff-Love displacements are expressed by *generator functions* $\boldsymbol{\zeta}$ with three components $(\zeta_1,\ \zeta_2,\ \zeta_3)^T(\boldsymbol{x}_*)$ only depending on in-plane variables, namely the membrane ones are generated by $\boldsymbol{\zeta}_* = (\zeta_1, \zeta_2)$ and the bending ones by ζ_3. We agree to denote

$$U_\mathrm{m}^\mathrm{KL}(\boldsymbol{\zeta}_*)(\boldsymbol{x}) \ \stackrel{\mathrm{def}}{=}\ \big(\zeta_1(\boldsymbol{x}_*), \zeta_2(\boldsymbol{x}_*), 0\big) \tag{2.4}$$

$$\begin{aligned}
U_\mathrm{b}^\mathrm{KL}(\zeta_3)(\boldsymbol{x}) &\stackrel{\mathrm{def}}{=} \Big(-X_3\partial_1\zeta_3(\boldsymbol{x}_*), -X_3\partial_2\zeta_3(\boldsymbol{x}_*), \frac{1}{\varepsilon}\,\zeta_3(\boldsymbol{x}_*)\Big) \qquad (2.5)\\
&= \frac{1}{\varepsilon}\big(-x_3\partial_1\zeta_3(\boldsymbol{x}_*), -x_3\partial_2\zeta_3(\boldsymbol{x}_*), \zeta_3(\boldsymbol{x}_*)\big).
\end{aligned}$$

Though containing ε, definition (2.5) reveals to be the most convenient one. Note that the *scaled* displacement $\widetilde{U}_{\mathrm{b}}^{\mathrm{KL}}(\zeta_3)$ is *independent of* ε. We denote in a natural way

$$U^{\mathrm{KL}}(\boldsymbol{\zeta}) \stackrel{\mathrm{def}}{=} U_{\mathrm{m}}^{\mathrm{KL}}(\boldsymbol{\zeta}_*) + U_{\mathrm{b}}^{\mathrm{KL}}(\zeta_3).$$

Under assumptions (2.2)-(2.3), the displacement solution of (2.1) can be expanded as:

$$\boldsymbol{u} \simeq U^{\mathrm{KL}}(\boldsymbol{\zeta}^0) + \varepsilon\big(U^{\mathrm{KL}}(\boldsymbol{\zeta}^1) + \boldsymbol{v}^1 + \boldsymbol{\varphi}^1\big) + \cdots + \varepsilon^k\big(U^{\mathrm{KL}}(\boldsymbol{\zeta}^k) + \boldsymbol{v}^k + \boldsymbol{\varphi}^k\big)\cdots \tag{2.6}$$

Remark. Compared to the general expansion (1.1), we see that $\boldsymbol{u}^0$ can be identified to $U^{\mathrm{KL}}(\boldsymbol{\zeta}^0)$, and for any $k \geq 1$, $\boldsymbol{u}^k$ is identified to the sum $U^{\mathrm{KL}}(\boldsymbol{\zeta}^k) + \boldsymbol{v}^k + \boldsymbol{\varphi}^k$.

Thus the expansions of the bending and membrane parts are:

$$\boldsymbol{u}_{\mathrm{b}} \simeq U_{\mathrm{b}}^{\mathrm{KL}}(\zeta_3^0) + \varepsilon\big(U_{\mathrm{b}}^{\mathrm{KL}}(\zeta_3^1) + \boldsymbol{v}_{\mathrm{b}}^1 + \boldsymbol{\varphi}_{\mathrm{b}}^1\big) + \varepsilon^2\big(U_{\mathrm{b}}^{\mathrm{KL}}(\zeta_3^2) + \boldsymbol{v}_{\mathrm{b}}^2 + \boldsymbol{\varphi}_{\mathrm{b}}^2\big) + \cdots \tag{2.7}$$

$$\boldsymbol{u}_{\mathrm{m}} \simeq U_{\mathrm{m}}^{\mathrm{KL}}(\boldsymbol{\zeta}_*^0) + \varepsilon\big(U_{\mathrm{m}}^{\mathrm{KL}}(\boldsymbol{\zeta}_*^1) + \boldsymbol{v}_{\mathrm{m}}^1 + \boldsymbol{\varphi}_{\mathrm{m}}^1\big) + \varepsilon^2\big(U_{\mathrm{m}}^{\mathrm{KL}}(\boldsymbol{\zeta}_*^2) + \boldsymbol{v}_{\mathrm{m}}^2 + \boldsymbol{\varphi}_{\mathrm{m}}^2\big) + \cdots \tag{2.8}$$

Therefore the leading terms modulo $\mathcal{O}(\varepsilon^2)$ in the expansion (2.7)-(2.8) are as follows:

$$\boldsymbol{u}_{\mathrm{b}} = \begin{pmatrix} -X_3\partial_1\zeta_3^0 - \varepsilon X_3\partial_1\zeta_3^1 + \ 0 \ + & 0 \\ -X_3\partial_2\zeta_3^0 - \varepsilon X_3\partial_2\zeta_3^1 + \ 0 \ + & 0 \\ \frac{1}{\varepsilon}\zeta_3^0 \quad + \quad \zeta_3^1 \quad + \varepsilon\zeta_3^2 + & \varepsilon\frac{\nu}{6(1-\nu)}(3X_3^2 - 1)\,\Delta_*\zeta_3^0 \end{pmatrix} + \varepsilon\boldsymbol{\varphi}_{\mathrm{b}}^1 + \mathcal{O}(\varepsilon^2) \tag{2.9}$$

$$\boldsymbol{u}_{\mathrm{m}} = \begin{pmatrix} \zeta_1^0 & + & \varepsilon\zeta_1^1 & + & 0 \\ \zeta_2^0 & + & \varepsilon\zeta_2^1 & + & 0 \\ 0 & + & 0 & - & \varepsilon\frac{\nu}{1-\nu}X_3\,\mathrm{div}_*\,\boldsymbol{\zeta}_*^0 \end{pmatrix} + \varepsilon\boldsymbol{\varphi}_{\mathrm{m}}^1 + \mathcal{O}(\varepsilon^2)\,, \tag{2.10}$$

where the symbol $\mathcal{O}(\varepsilon^2)$ means that the remainder is uniformly bounded by $c\varepsilon^2$.

Remark. The displacements $\boldsymbol{v}^1$ with zero integral mean value appear in (2.9) and (2.10) as

$$\boldsymbol{v}_{\mathrm{b}}^1(\boldsymbol{x}_*, X_3) = \frac{\nu}{6(1-\nu)}\Big(0,\ 0,\ (3X_3^2 - 1)\,\Delta_*\zeta_3^0\Big)^T, \tag{2.11}$$

$$\boldsymbol{v}_{\mathrm{m}}^1(\boldsymbol{x}_*, X_3) = \frac{\nu}{1-\nu}\Big(0,\ 0,\ -X_3\,\mathrm{div}_*\,\boldsymbol{\zeta}_*^0\Big)^T. \tag{2.12}$$

They are in fact completely determined by $\boldsymbol{\zeta}^0$.

Remark. In the hard-clamped case the first membrane boundary-layer term $\boldsymbol{\varphi}_{\mathrm{m}}^1$, resp. bending $\boldsymbol{\varphi}_{\mathrm{b}}^1$, is only present if $\mathrm{div}_*\,\boldsymbol{\zeta}_*^0$ is non-zero on $\partial\omega$, resp. $\Delta_*\zeta_3^0 \neq 0$ on $\partial\omega$. In the free situation $\boldsymbol{\varphi}^1 \equiv \boldsymbol{\varphi}_{\mathrm{b}}^1$ and $\boldsymbol{\varphi}^1$ is present only if $(\partial_n + \kappa)\partial_s\zeta_3^0$ is non-zero on $\partial\omega$. Visualization of these profiles is provided in [7].

2.4 Membrane and bending equations for the generators

The generator functions $\boldsymbol{\zeta}_*^k$ and ζ_3^k are defined on ω and they are solutions to the following problems. $\boldsymbol{\zeta}_*^k$ is solution of the "membrane equation":

$$\mu\,\Delta_*\boldsymbol{\zeta}_*^k + (\tilde{\lambda}+\mu)\nabla_*\,\mathrm{div}_*\,\boldsymbol{\zeta}_*^k = \boldsymbol{R}_{\mathrm{m}}^k\,, \tag{2.13}$$

whereas ζ_3^k solves the "bending equation":

$$(\tilde{\lambda}+2\mu)\Delta_*^2\zeta_3^k = R_{\mathrm{b}}^k \tag{2.14}$$

with $\tilde{\lambda} = 2\lambda\mu(\lambda+2\mu)^{-1}$ and with right hand sides $\boldsymbol{R}_{\mathrm{m}}^k$ and R_{b}^k only depending on the data $\boldsymbol{f}$ and $\boldsymbol{t}^\pm$ in problem (2.1).

The right hand side of (2.13) for $\boldsymbol{\zeta}_*^0$ is given by:

$$\boldsymbol{R}_{\mathrm{m}}^0(\boldsymbol{x}_*) = -\frac{1}{2}\left[\int_{-1}^{+1}\boldsymbol{F}_*(\boldsymbol{x}_*,X_3)\,dX_3 + \boldsymbol{T}_*^+ + \boldsymbol{T}_*^-\right]$$

and the right hand side of (2.14) for ζ_3^0 is:

$$R_{\mathrm{b}}^0(\boldsymbol{x}_*) = \frac{3}{2}\left[\int_{-1}^{+1}F_3\,dX_3 + T_3^+ + T_3^- + \mathrm{div}_*\Big(\int_{-1}^{+1}X_3\,\boldsymbol{F}_*\,dX_3 + \boldsymbol{T}_*^+ - \boldsymbol{T}_*^-\Big)\right]\,.$$

For $k=1$, we have simply $\boldsymbol{R}_{\mathrm{m}}^1 = 0$ and $R_{\mathrm{b}}^1 = 0$, whereas for $k=2$ formulas are much more involved and require the introduction of several new notations. For the sake of completeness, we simply quote them from [3].

Let $[F]_m$ denote the m-th moment with respect to X_3 of F:

$$[F]_m = \int_{-1}^{+1} X_3^m\,F(\boldsymbol{x}_*,X_3)\,dX_3$$

and let us introduce the primitives

$$\oint^{X_3} F\,dY_3 \;:=\; \int_{-1}^{X_3} F(Y_3)\,dY_3 - \frac{1}{2}\int_{-1}^{+1}\int_{-1}^{Z_3} F(Y_3)\,dY_3\,dZ_3,$$

$$\fint^{Y_3} F\,dZ_3 \;:=\; \frac{1}{2}\left(\int_{-1}^{Y_3} F(Z_3)\,dZ_3 - \int_{Y_3}^{+1} F(Z_3)\,dZ_3\right).$$

Now we need two functions of the data $(\boldsymbol{f},\boldsymbol{t}^\pm)$: $\boldsymbol{\mathfrak{G}}$ and $\boldsymbol{\mathfrak{H}}$. These functions are part of formulas giving not only the right hand sides for $\boldsymbol{\zeta}^2$, see (2.18), but also the first non-zero term in the presence of a higher-order response, see §3. In the examples that we illustrate, the relevant components of $\boldsymbol{\mathfrak{G}}(\boldsymbol{f},\boldsymbol{t}^\pm)$ and $\boldsymbol{\mathfrak{H}}(\boldsymbol{f},\boldsymbol{t}^\pm)$ are simple polynomial functions, see the corollaries in §3. The function $\boldsymbol{\mathfrak{G}} = \boldsymbol{\mathfrak{G}}(\boldsymbol{f},\boldsymbol{t}^\pm)$ is defined in $\mathcal{C}^\infty(\overline{\omega}\times[-1\,,\,1])^3$ by

$$\mathfrak{G}_3 = 0 \quad\text{and}\quad \boldsymbol{\mathfrak{G}}_*(x_*,X_3) = -\frac{1}{\mu}\left(\oint^{X_3}\Big(\fint^{Y_3}\boldsymbol{F}_*\Big)\,dY_3 - X_3\,\frac{\boldsymbol{T}_*^+ - \boldsymbol{T}_*^-}{2}\right). \tag{2.15}$$

The function $\boldsymbol{\mathfrak{H}} = \boldsymbol{\mathfrak{H}}(\boldsymbol{f}, \boldsymbol{t}^{\pm})$ is defined in $\mathcal{C}^{\infty}(\overline{\omega} \times [-1\,,\,1])^3$ by

$$\mathfrak{H}_3 = -\frac{1}{\lambda+2\mu}\left(\oint^{X_3}\Big(\int\!\!\!\!\!\!-^{Y_3} F_3\Big)\,dY_3 - X_3\,\frac{T_3^+ - T_3^-}{2}\right) \quad \text{and}$$

$$\mathfrak{H}_\alpha = -\oint^{X_3}\left(\partial_\alpha\mathfrak{H}_3 + \frac{1}{\mu}\,Y_3\,\mathfrak{F}_\alpha(\boldsymbol{\mathfrak{G}}) + \frac{\lambda}{\mu}\int\!\!\!\!\!\!-^{Y_3}\left\{\partial_{\alpha 3}\mathfrak{H}_3 - \frac{1}{2}\int_{-1}^{+1}\partial_{\alpha 3}\mathfrak{H}_3\,dZ_3\right\}\right)dY_3\,, \tag{2.16}$$

where the operator $\boldsymbol{\mathfrak{F}}\,:\,\boldsymbol{v}\mapsto\boldsymbol{\mathfrak{F}}(\boldsymbol{v})$ is defined from $\mathcal{C}^{\infty}(\overline{\omega} \times [-1\,,\,1])^3$ into $\mathcal{C}^{\infty}(\overline{\omega})^3$ by

$$\mathfrak{F}_\alpha(\boldsymbol{v}) = \frac{\tilde\lambda}{2}\int_{-1}^{+1}\int\!\!\!\!\!\!-^{Y_3}\partial_{\alpha\beta}e_{\beta 3}(\boldsymbol{v})\;dZ_3\,dY_3 \quad \text{and} \quad \mathfrak{F}_3(\boldsymbol{v}) = \mu\int_{-1}^{+1}\partial_\beta e_{\beta 3}(\boldsymbol{v})\;dY_3. \tag{2.17}$$

Finally the right hand sides of equations (2.13) and (2.14) for $k=2$ are given by

$$\boldsymbol{R}^2_{\mathrm{m}} = \boldsymbol{\mathfrak{F}}_*(\boldsymbol{\mathfrak{G}}) - \frac{\tilde\lambda}{4\mu}\nabla_*\left([F_3]_1 + T_3^+ - T_3^-\right) \quad \text{and}$$
$$R^2_{\mathrm{b}} = 3\mathfrak{F}_3(\boldsymbol{\mathfrak{H}}) + \frac{3\mu(3\lambda+4\mu)}{2(\lambda+2\mu)}\Delta_*\,\mathrm{div}_*[\boldsymbol{\mathfrak{G}}_*]_1. \tag{2.18}$$

2.5 Boundary conditions for the generators

The boundary conditions for the generators on $\partial\omega$ depend of course on the specified boundary conditions on the lateral face of the plate.

(i) FOR THE HARD CLAMPED PLATE: the boundary operators are the Dirichlet conditions associated with the membrane and bending operators in (2.13) and (2.14). For $k=0$ and 1, the boundary conditions are:

$\zeta^0_3 = 0,\ \partial_n\zeta^0_3 = 0$ for the bending equation and $\boldsymbol{\zeta}^0_* = \boldsymbol{0}$ for the membrane equation.

$\zeta^1_n = c_1\,\mathrm{div}_*\,\boldsymbol{\zeta}^0_*\,,\ \zeta^1_s = 0\,,$ for the membrane equation and $\zeta^1_3 = 0\,,\ \partial_n\zeta^1_3 = c_2\,\Delta_*\zeta^0_3\,,$ for the bending equation, where $c_1 = c_1(\lambda,\mu)$ and $c_2 = c_2(\lambda,\mu)$ are non-zero universal coefficients.

(ii) FOR THE FREE PLATE: the boundary operators are the Neumann conditions associated with the correct bilinear forms corresponding to the membrane and bending operators in (2.13) and (2.14).

For $k=0$ these are: For the membrane equation

$$\mu(\partial_s\zeta^0_n + \partial_n\zeta^0_s + 2\kappa\zeta^0_s) \;=\; 0 \tag{2.19}$$
$$\tilde\lambda\,\mathrm{div}_*\,\boldsymbol{\zeta}^0_* + 2\mu\partial_n\zeta^0_n \;=\; 0 \tag{2.20}$$

and for the bending equation

$$\tilde\lambda\Delta_*\zeta^0_3 + 2\mu\partial_{nn}\zeta^0_3 \;=\; 0 \tag{2.21}$$
$$(\tilde\lambda+2\mu)\partial_n\Delta_*\zeta^0_3 + 2\mu\partial_s(\partial_n+\kappa)\partial_s\zeta^0_3 \;=\; \frac{3}{2}\left[\int_{-1}^{+1}X_3\,F_n\,dX_3 + T_n^+ - T_n^-\right], \tag{2.22}$$

where κ denotes the curvature of $\partial\omega$. The generating function $\boldsymbol{\zeta}^1$ satisfies homogeneous boundary conditions like $\boldsymbol{\zeta}^0$ in (2.19)-(2.20). Since equation (2.13) for $\boldsymbol{\zeta}^1_*$ is also homogeneous, then $\boldsymbol{\zeta}^1_*$ is identically zero.

For the bending equation

$$\tilde{\lambda}\Delta_*\zeta_3^1 + 2\mu\partial_{nn}\zeta_3^1 = c_3\,\partial_s(\partial_n+\kappa)\partial_s\zeta_3^0 \tag{2.23}$$

$$(\tilde{\lambda}+2\mu)\partial_n\Delta_*\zeta_3^1 + 2\mu\partial_s(\partial_n+\kappa)\partial_s\zeta_3^1 = d(s) \tag{2.24}$$

where $c_3 = c_3(\lambda,\mu)$ is a universal coefficient and $d(s)$ depends on special traces of ζ_3^0 as well as on F_n and $T_n^{\pm}$.

3 HIGHER ORDER RESPONSES

Under special loading conditions, which will be described in the sequel, the leading term in the expansion (2.6) vanish, i.e. the generator $\boldsymbol{\zeta}^0 \equiv \mathbf{0}$, providing a displacement field of higher order. We agree to define the order of the response according to:

Definition 3.1 With the assumptions (2.2)-(2.3) and if $\boldsymbol{\zeta}^0 \equiv \mathbf{0}$, we call *order of the response* the smallest integer k such that at least one of the three terms $\boldsymbol{\zeta}^k$, $\boldsymbol{v}^k$ or $\boldsymbol{\varphi}^k$ involved in expansion (2.6) is not zero. ■

Readers interested in more detailed proofs of the results stated herein are referred to [12]. The displacement asymptotic expansion for hard clamped plates is first considered followed by free plate lateral boundary conditions. We also highlight the difference in the higher-order responses due to the different lateral boundary conditions.

3.1 Hard clamped plates

From equations (2.13)-(2.14) for $\boldsymbol{\zeta}^0$ and the associated homogeneous boundary conditions, it is clear that if $\boldsymbol{R}^0_{\mathrm{m}}$ and R^0_{b} are zero, then $\boldsymbol{\zeta}^0 \equiv \mathbf{0}$. In this case, as $\boldsymbol{R}^1_{\mathrm{m}}$ and R^1_{b} are zero too and the boundary data of $\boldsymbol{\zeta}^1$ depends linearly on $\boldsymbol{\zeta}^0$, we also have $\boldsymbol{\zeta}^1 \equiv \mathbf{0}$. Formulas (2.11)-(2.12) yield that $\boldsymbol{v}^1 \equiv \mathbf{0}$. Moreover, as $\boldsymbol{\varphi}^1$ also depends linearly on $\boldsymbol{\zeta}^0$, it is zero too. Thus the order of the response is at least 2.

Theorem 3.2 [3] *For any loading $(\boldsymbol{f},\boldsymbol{t}^{\pm})$ such that $\boldsymbol{R}^0_{\mathrm{m}} = \mathbf{0}$ and $R^0_{\mathrm{b}} = 0$, and that either $\boldsymbol{R}^2_{\mathrm{m}}$ or R^2_{b} or $\mathfrak{G}(\boldsymbol{f},\boldsymbol{t}^{\pm})$ is not identically zero, the order of the response is 2. The first non-zero term in the expansion* (2.6) *of $\boldsymbol{u}$ is*

$$\varepsilon^2\Big(U^{\mathrm{KL}}(\boldsymbol{\zeta}^2) + \underbrace{\mathfrak{G}_*(\boldsymbol{f},\boldsymbol{t}^{\pm})}_{=\boldsymbol{v}^2} + \boldsymbol{\varphi}^2\Big). \tag{3.1}$$

As corollaries of Theorem 3.2 we exhibit special load conditions to excite order 2 responses in bending and membrane solutions.

Corollary 3.3 [3] *Let* $f_3 = t_3^\pm = 0$, $\boldsymbol{f}_* = -3X_3(1,\ 1)^T$, $\boldsymbol{t}_*^+ = (\varepsilon,\ \varepsilon)^T$ *and* $\boldsymbol{t}_*^- = -(\varepsilon,\ \varepsilon)^T$ *representing a bending load. Then we have an order* 2 *response and the expansion of the displacement* $\boldsymbol{u} = \boldsymbol{u}_\mathrm{b}$ *starts like:*

$$\boldsymbol{u}_\mathrm{b} = \varepsilon^2 \left[\begin{pmatrix} -X_3\partial_1\zeta_3^2 & + & 0 & + & \mathfrak{G}_1 \\ -X_3\partial_2\zeta_3^2 & + & 0 & + & \mathfrak{G}_2 \\ \frac{1}{\varepsilon}\zeta_3^2 & + & \zeta_3^3 & + & 0 \end{pmatrix} + \boldsymbol{\varphi}_\mathrm{b}^2 + \mathcal{O}(\varepsilon) \right] \tag{3.2}$$

with $\mathfrak{G}_1 = \mathfrak{G}_2 = (2\mu)^{-1}(X_3^3 - X_3)$.

Corollary 3.4 [3] *Let* $f_3 = t_3^\pm = 0$, $\boldsymbol{f}_* = -(1,\ 1)^T$, $\boldsymbol{t}_*^\pm = (\varepsilon,\ \varepsilon)^T$ *representing a membrane load. Then we have an order* 2 *response and the expansion of* $\boldsymbol{u} = \boldsymbol{u}_\mathrm{m}$ *starts like:*

$$\boldsymbol{u}_\mathrm{m} = \varepsilon^2 \left[\begin{pmatrix} \zeta_1^2 & + & \mathfrak{G}_1 \\ \zeta_2^2 & + & \mathfrak{G}_2 \\ & 0 & \end{pmatrix} + \boldsymbol{\varphi}_\mathrm{m}^2 + \mathcal{O}(\varepsilon) \right] \tag{3.3}$$

with $\mathfrak{G}_1 = \mathfrak{G}_2 = (3\mu)^{-1}(3X_3^2 - 1)$.

We may have higher orders than 2:

Theorem 3.5 [3] *For any loading case which satisfies* $(\boldsymbol{f}_*,\ \boldsymbol{t}_*^\pm) = \boldsymbol{0}$ *and*

$$\left([F_3]_0 + T_3^+ + T_3^-\right) = \nabla_* \left([F_3]_1 + T_3^+ - T_3^-\right) = \Delta_* \left([F_3]_2 - [F_3]_0\right) = 0 \ \ in\,\omega$$

then $\boldsymbol{R}_\mathrm{m}^0 = \boldsymbol{R}_\mathrm{m}^2 = R_\mathrm{b}^0 = R_\mathrm{b}^2 = 0$ *and* $\mathfrak{G}(\boldsymbol{f}, \boldsymbol{t}^\pm) = \boldsymbol{0}$, *and the order of the answer is* ≥ 3.

As corollaries of Theorem 3.5 we exhibit special load conditions to excite order 3 responses in bending and membrane solutions. Then first non-zero term in the expansion (2.6) of $\boldsymbol{u}$ is

$$\varepsilon^3 \Big(U^{\mathrm{KL}}(\boldsymbol{\zeta}^3) + \underbrace{\big(\boldsymbol{0}, \mathfrak{H}_3(\boldsymbol{f}, \boldsymbol{t}^\pm)\big)}_{=\,\boldsymbol{v}^3} + \boldsymbol{\varphi}^3 \Big). \tag{3.4}$$

Corollary 3.6 [3] *Let* $f_3 = \varepsilon(X_3^2 - 1/3)$ *and* $t_3^\pm = 0$. *Then we have an order* 3 *response and the expansion of the displacement* $\boldsymbol{u} = \boldsymbol{u}_\mathrm{b}$ *starts like:*

$$\boldsymbol{u}_\mathrm{b} = \varepsilon^3 \left[\begin{pmatrix} -X_3\partial_1\zeta_3^3 & + & 0 & + & 0 \\ -X_3\partial_2\zeta_3^3 & + & 0 & + & 0 \\ \frac{1}{\varepsilon}\zeta_3^3 & + & \zeta_3^4 & + & \mathfrak{H}_3 \end{pmatrix} + \boldsymbol{\varphi}_\mathrm{b}^3 + \mathcal{O}(\varepsilon) \right]. \tag{3.5}$$

Here $\mathfrak{H}_3$ *is a non-zero even polynomial of degree 4 in* X_3.

Corollary 3.7 *Let* $f_3 = \varepsilon$, $t_3^\pm = -\varepsilon^2$. *Then we have an order* 3 *response and the expansion of the displacement* $\boldsymbol{u} = \boldsymbol{u}_\mathrm{b}$ *starts like in* (3.5).

Corollary 3.8 [3] *Let* $f_3 = 0$, $t_3^+ = \varepsilon^2$ *and* $t_3^- = -\varepsilon^2$. *Then we have an order* 3 *response and the expansion of the displacement* $\boldsymbol{u} = \boldsymbol{u}_{\mathrm{m}}$ *starts like*

$$\boldsymbol{u}_{\mathrm{m}} = \varepsilon^3 \left[\begin{pmatrix} \zeta_1^3 & + & 0 \\ \zeta_2^3 & + & 0 \\ 0 & + & \mathfrak{H}_3 \end{pmatrix} + \boldsymbol{\varphi}_{\mathrm{m}}^2 + \mathcal{O}(\varepsilon) \right]. \tag{3.6}$$

with $\mathfrak{H}_3 = (\lambda + 2\mu)^{-1} X_3$.

Remark. There exist loads $\boldsymbol{f}$ and $\boldsymbol{t}^{\pm}$ which may generate fourth order response. Specific loadings for this case can be found in [3]. But if the loads are not identically zero and satisfy (2.2)-(2.3), we cannot have order 5 responses or larger.

3.2 Free plates

Theorem 3.9 [2] *For any loading* $\boldsymbol{f}$ *and* $\boldsymbol{t}^{\pm}$ *such that* $\boldsymbol{R}_{\mathrm{m}}^0 = \boldsymbol{0}$, $R_{\mathrm{b}}^0 = 0$ *in* ω *and* $\frac{3}{2}\left[\int_{-1}^{+1} X_3\, f_n\, dX_3 + T_n^+ - T_n^-\right] = 0$ *on* $\partial\omega$, *the order of the response is* ≥ 2. *If either* $\boldsymbol{R}_{\mathrm{m}}^2$ *or* R_{b}^2 *or* $\mathfrak{G}(\boldsymbol{f}, \boldsymbol{t}^{\pm})$ *or one of the boundary conditions for* $\boldsymbol{\zeta}^2$ *is not identically zero, then the order of the response is* 2 *and the expansion of* $\boldsymbol{u}$ *starts like in* (3.2)-(3.3).

Theorem 3.10 [2] *The order of the response is* ≥ 3 *if and only if the generators* $\boldsymbol{\zeta}^k \equiv 0$, $k = 0, 1, 2$, *and additionally* $\mathfrak{G}(\boldsymbol{f}, \boldsymbol{t}^{\pm}) = \boldsymbol{0}$. *This is exactly the case if* $\boldsymbol{f}_* = \boldsymbol{t}_*^{\pm} = \boldsymbol{0}$ *and*

$$\left([F_3]_0 + T_3^+ + T_3^-\right) = \left([F_3]_1 + T_3^+ - T_3^-\right) = \left([F_3]_2 - [F_3]_0\right) = 0 \ \ in\, \omega\,.$$

Then the expansion of $\boldsymbol{u}$ *starts like in* (3.5)-(3.6).

Comparing Theorem 3.10 (for the free plate) with Theorem 3.5 (for the hard clamped plate) one notices that if a loading produces an order 3 response for the free plate then the same loading will produce a higher-order response for the hard clamped plate as well, but contrary there exist loadings which produce a higher-order response in the hard-clamped plate and does not produce it in the free plate, see [12].

4 NUMERICAL VISUALIZATION OF HIGHER-ORDER RESPONSES

The theoretical results are visualized by computing functionals associated with the displacement field for free and hard clamped lateral boundary conditions, and for various loadings exciting the higher order terms. The computations are done within the finite element code Stress Check.* We consider a rectangular plate with dimensions $4 \times 1 \times 2\varepsilon$ as shown in Figure 2. The material properties are: Poisson ratio $\nu = 1/8$ and Young modulus $E = 27/4$. All lateral boundary conditions are either free or hard clamped, thus there are two axes of symmetry, so that only a quarter of the plate may be analyzed, namely plate $ABCG$, with symmetry boundary conditions on AG and GC.

* Stress Check is a trade mark of Engineering Software Research and Development, Inc., 10845 Olive Blvd., Suite 170, St. Louis, MO 63141, USA

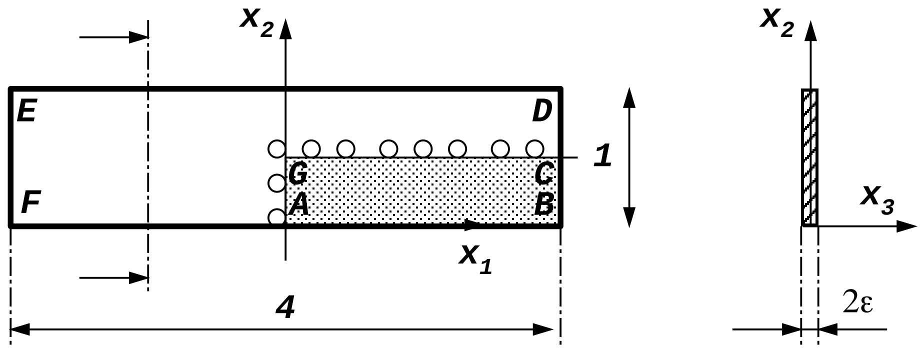

Figure 2: *Rectangular plate under consideration.*

A three dimensional p-version finite element model is constructed having two elements in the thickness direction, four elements in the x_2 direction and six elements in the x_1 direction. In the neighborhood of the edges, the mesh is graded so that there are two elements of dimension ε each. See Figure 3 for a typical mesh for $2\varepsilon = 0.1$ and Figure 4 for $2\varepsilon = 0.001$ and hard clamped lateral boundary conditions. The finite element

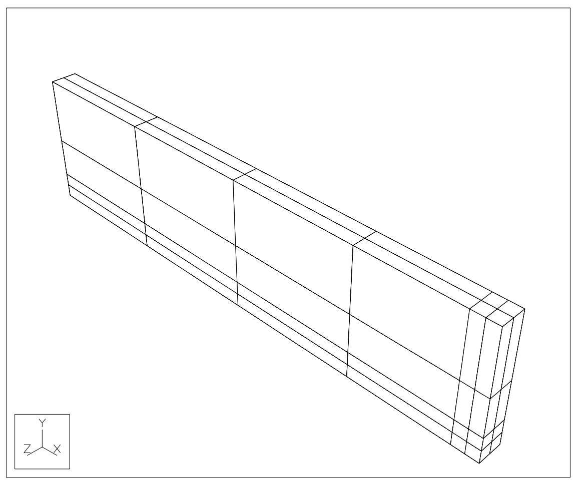

Figure 3: *Finite element mesh for the plate with* $2\varepsilon = 0.1$.

model is constructed parametrically so that the value of 2ε may vary, and we change it from 0.1 ($= 10^{-1}$) to 0.001 ($= 10^{-3}$). Although not visible in Figure 4, there are two elements across the thickness and two elements each of dimension ε in the neighborhood of the boundary. The p-level over each element has been increased from 1 to 8 and the trunk space has been used (see [13]). There are 12,568 degrees of freedom at $p = 8$. An advantage of using p-version finite element methods is this possibility of having “needle elements” in the boundary layer zone with aspect ratios as large as 10,000 without significant degradation in the numerical performance. An *exponential convergence rate* is obtained without thickness-locking phenomenon visible (due to the use of high-order elements) and the convergence of the computed data has been examined as well for increasing p-levels in order to evaluate the reliability of the numerical results.

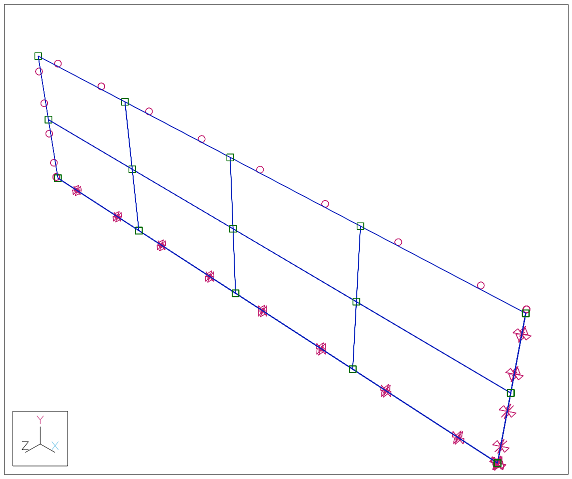

Figure 4: *Finite element mesh and boundary conditions for the plate with* $2\varepsilon = 0.001$.

By considering (2.7)-(2.8), one notices that in the generic case the displacement field is dominated by the Kirchhoff-Love components, in particular the transversal bending component of $U_{\rm b}^{\rm KL}(\zeta_3^0)$ is much larger than any other component of the displacement. In contrast to that, for the higher-order responses the operators $\mathfrak{G}$ and $\mathfrak{H}$ play an important role in the expansion of the displacement field, see (3.1)-(3.3) and (3.4)-(3.6). In order to be able to visualize single terms in the expansion for the considered examples and in particular to extract constants with respect to X_3 as well as expressions with vanishing integral mean value, we introduce for $j = 1, 2, 3$ and $i, m \in \mathbb{N}$ the following quantities

$$J_m[u_j, P_i] = \frac{1}{(2\varepsilon)^m} \int_{-1}^{+1} u_j(\boldsymbol{x}_*, X_3) P_i(X_3)\, dX_3 \,, \tag{4.1}$$

where P_i is the i-th Legendre polynomial. Since $\boldsymbol{\zeta}^k$ are constants in X_3 then they are L_2-orthogonal to P_i ($i \neq 0$). In contrast to that, the expressions $\boldsymbol{v}^k$ are orthogonal to P_0. Based on the parity properties of the membrane and bending parts, the quantities $J_m[u_j, P_i]$ vanish either for all even or for all odd values of i depending on the type and on the component of the displacement field under consideration. The quantities in (4.1) will enable us to visualize in the higher-order response, the single parts in the leading terms and in particular to make the appearing boundary layer effects visible.

4.1 Hard clamped plate, bending response of order 3

The first example which we consider should be understood as a motivating example in order to indicate the existence of higher-order responses and their significance. The loadings for this example read: $f_\alpha = 0$, $t_\alpha^\pm = 0$, $f_3 = \varepsilon$, $t_3^\pm = -\gamma\varepsilon^2$ with γ a real parameter. In the following we are going to change γ such that the existence of a higher-order response will be visible. For $\gamma = 1$, the loading is as in Corollary 3.7, thus one expects u_3 to behave as ε^2 as $\varepsilon \to 0$. For any other $\gamma \neq 1$, the “bending” solution, with the Kirchhoff-Love vertical component $u_3 \to \infty$ like $1/\varepsilon$ is expected as $\varepsilon \to 0$.

To be able to obtain a global information about the behavior of the displacement field we introduce a global L_2-norm (on the whole plate)

$$I(u_j) = \sqrt{\frac{1}{2\varepsilon}\int_\Omega |u_j|^2 \, dx_1 \, dx_2 \, dx_3}. \tag{4.2}$$

We expect that for $\gamma \neq 1$ and for $\varepsilon \to 0$, $I(u_3)$ tends to infinity with an order $\mathcal{O}(\varepsilon^{-1})$ as predicted by (2.7), but for $\gamma = 1$, $I(u_3)$ will converge to zero with an order $\mathcal{O}(\varepsilon^2)$. This should also have some influence for γ close to one, but the change for $I(u_3)$ from tending to infinity with an order $\mathcal{O}(\varepsilon^{-1})$ to tending to zero with an order $\mathcal{O}(\varepsilon^2)$ should be smooth (with maybe high gradients) with respect to the change of γ near $\gamma = 1$. Indeed, as expected by the mathematical analysis, the numerical results shown in Figure 5 demonstrate this behavior.

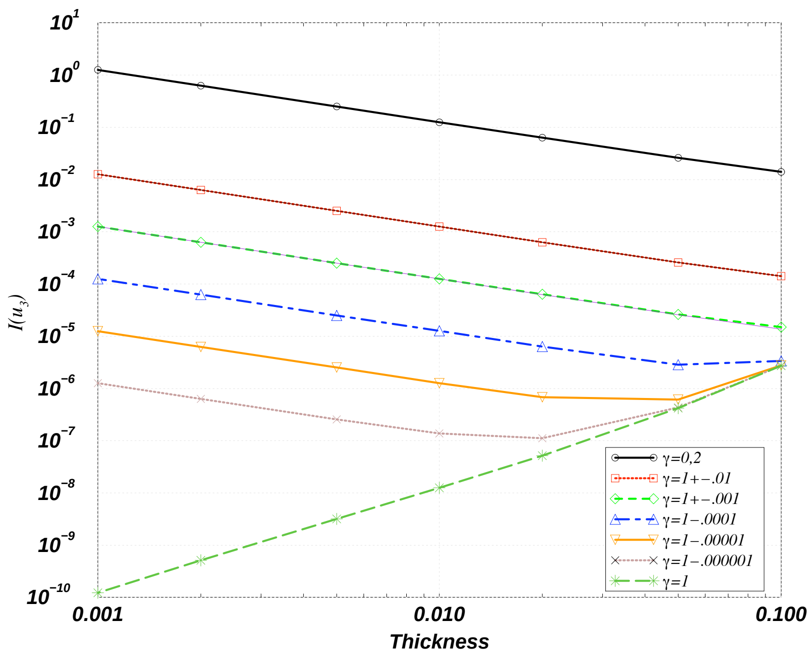

Figure 5: $I(u_3)$ *for various* γ *as* $2\varepsilon \to 0$.

4.2 Hard clamped plate, bending response of order 2

The second example which we consider is a bending example and the loadings are the following: $f_1 = f_2 = -3X_3$, $f_3 = 0$, $t_1^\pm = t_2^\pm = \pm\varepsilon$, $t_3^\pm = 0$. This loading according to Corollary 3.3 produces an order 2 response.

In Figure 6 we present the functional $J_2[u_3, P_2]$ along the line $x_1 = 1$, $0 \leq x_2 \leq 0.15$, i.e. with respect to the *physical* distance to the lateral boundary. Since P_2 is orthogonal to the constant (over the thickness) terms ζ_3^k, we expect that $J_2[u_3, P_2]$ will vary in

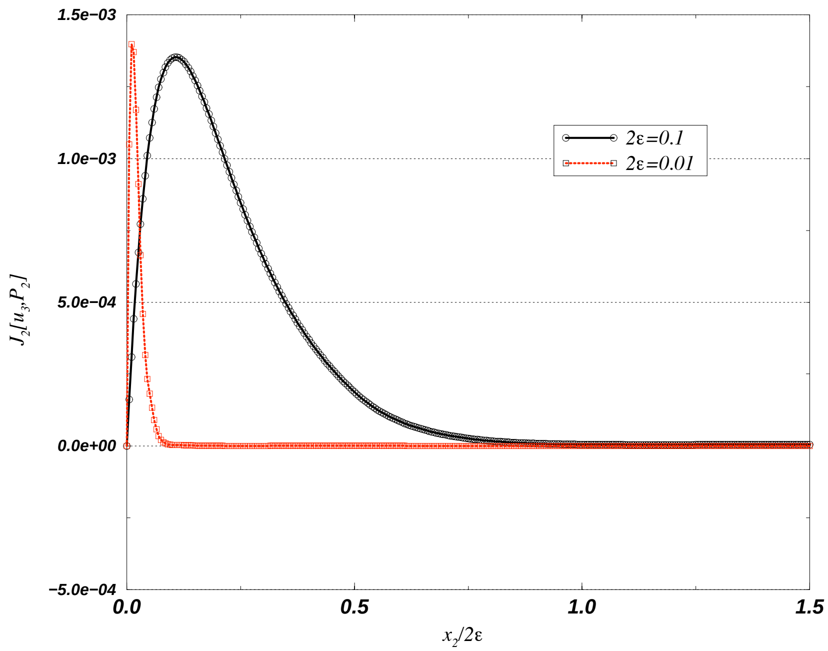

Figure 6: *Hard Clamped* $J_2[u_3, P_2]$.

the boundary layer zone only due to the presence of the boundary layer term $\varphi^2_{\mathrm{b},3}$ in the leading term of the asymptotic expansion and then will vanish as we move inside the plate. We moreover expect to see how the width of the boundary layer varies in dependence of ε , since we have chosen a representation in the physical variable. It can be noticed that indeed the boundary layer is only active in a strip of a width of order ε in the vicinity of the lateral boundary.

However such an evaluation does not allow a comparison of the single functionals $J_2[u_3, P_2]$ for different values of ε in the boundary layer zone. That is the reason why in the following the functionals $J_m[u_j, P_i]$ are always evaluated with respect to the stretched distance $x_2/2\varepsilon$. So we evaluate $J_m[u_j, P_i]$ on a set of equidistant points along the line $x_1 = 1$, $0 \leq x_2/2\varepsilon \leq 3$. We notice in this case, as shown in Figure 7, that the curves for different values of ε overlap, i.e they are independent of ε . Moreover, $J_2[u_3, P_2]$ is almost zero for $x_2/2\varepsilon > 1$, which manifests a rapidly decreasing profile. All of this is in accordance with the prediction of the mathematical analysis.

In Figure 8 we present $J_1[u_3, P_0]$ with respect to the physical variable x_2 . We expect to see ζ^2_3 only, since all the other terms are of higher order. Moreover, if we can see a boundary layer zone at all, it should be of width ε as in Figure 6. But as said above in order to be able to visualize the boundary layer behavior we are interested in the evaluation with respect to the stretched variable $x_2/2\varepsilon$, which we present in Figure 9.

Since $J_2[u_3, P_0]$ is nothing but the integral mean value of u_3 across the thickness, we now expect to see the influence of both ζ^2_3 and $\varphi^2_{\mathrm{b},3}$. At the first look one would expect

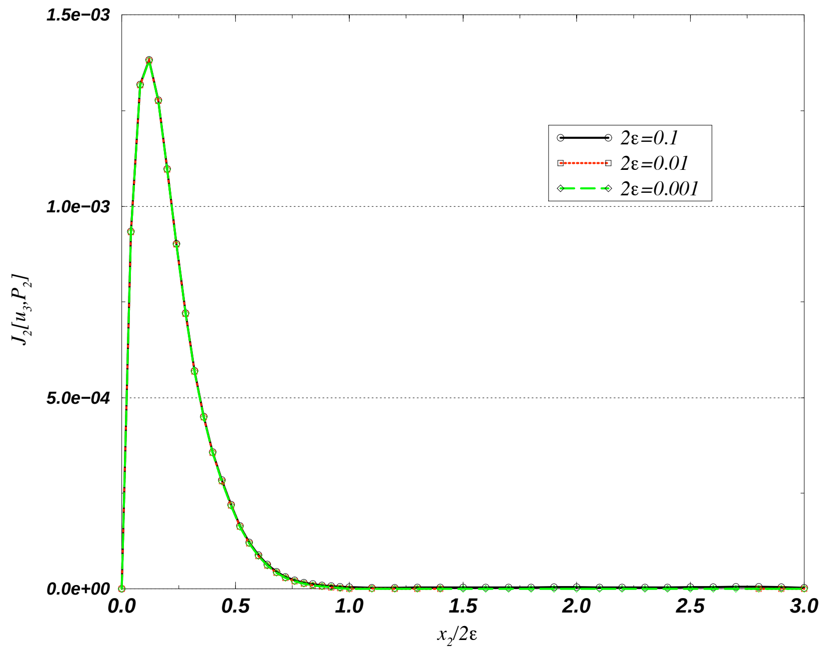

Figure 7: *Hard Clamped* $J_2[u_3, P_2]$ *vis. stretched distance.*

that because of the presence of ζ_3^2 in the asymptotic expansion $m = 1$ would hold and moreover, it would be $1/\varepsilon$ larger than $\varphi^2_{\mathrm{b},3}$. But as it can be seen from Figure 9 this is not true and $m = 2$ turns out to be the correct value. The reason for this is that we have evaluated $J_2[u_3, P_0]$ with respect to the stretched variable $x_2/2\varepsilon$, while ζ_3^2 in fact depends on the physical distance x_2. But, if one develops ζ_3^2 in its Taylor series with respect to x_2 around $x_2 = 0$, then in this series the constant (in x_2) vanishes because of the lateral Dirichlet condition $\zeta_3^2 = 0$ on $\partial\omega$, and the Taylor series starts with a linear (in x_2) part. Considering now the Taylor series of ζ_3^2 with respect to the stretched variable $x_2/2\varepsilon$ (around $x_2 = 0$), i.e. we replace any x_2 in the series above by $\varepsilon(x_2/\varepsilon)$, it turns out that the asymptotic expansion of u_3 indeed starts with ε^2, such that $m = 2$ is the correct choice. In Figure 9 there is almost no boundary layer behavior visible, which means that ζ_3^2 dominates $\varphi^2_{\mathrm{b},3}$.

In Figure 10 we visualize $J_2[u_1, P_1]$. We expect to see the influence of all the three terms $-X_3\partial_1\zeta_3^2$, $\mathfrak{G}_1$ and $\varphi^2_{\mathrm{b},1}$ which are contained in the leading term of the expansion. But in fact $J_2[u_1, P_1]$ varies in the boundary layer zone due to effect of the boundary layer profile $\varphi^2_{\mathrm{b},1}$ and becomes constant as we move away from the boundary inside the plate, which is the effect of $\mathfrak{G}_1$. Indeed, $J_2[u_1, P_1]$ tends to $-1/90$ in the interior of the plate which is the exact value of $J_2[\varepsilon^2\mathfrak{G}_1, P_1]$, i.e. $\varepsilon^2\mathfrak{G}_1$ represents the leading term in the expansion of u_1 outside the boundary layer zone. Here we recall that it holds $G_{\mathrm{b},\alpha} = (2\mu)^{-1}(X_3^3 - X_3)$, compare Corollary 3.3. The explanation why we cannot see $-X_3\partial_1\zeta_3^2$ is similar to the one in Figure 9. Since $x_1 \equiv s$ in the boundary layer zone, there $\partial_1\zeta_3^2$ coincides with $\partial_s\zeta_3^2$, which vanishes for $x_2 = 0$ because of the lateral Dirichlet

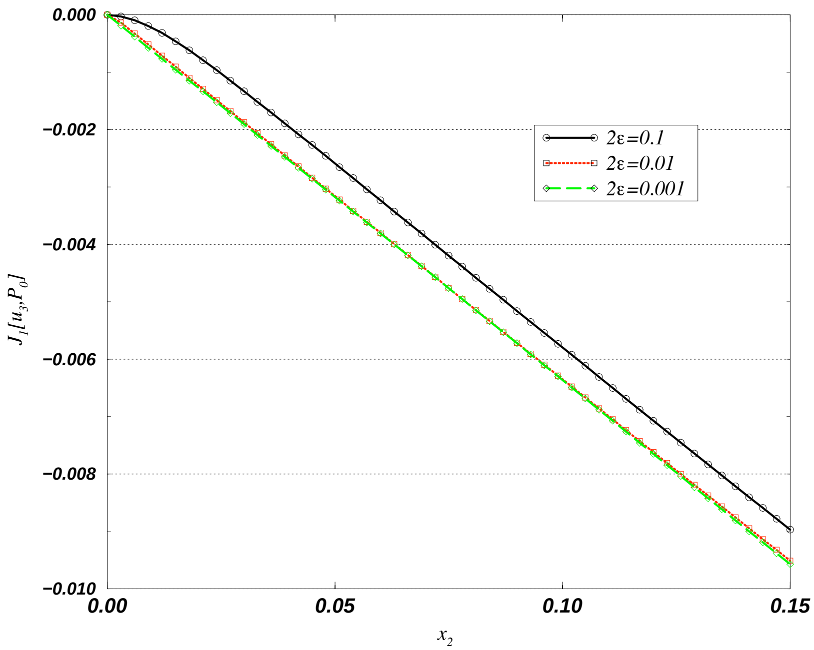

Figure 8: *Hard Clamped* $J_1[u_3, P_0]$.

condition $\zeta_3^2 = 0$ on $\partial\omega$. But this means that the Taylor series of $\partial_1\zeta_3^2$ in x_2 around $x_2 = 0$ starts with the linear term and hence the Taylor series in $x_2/2\varepsilon$ starts altogether with ε^3 and thus is in fact not present in the leading term.

In Figure 11 we present $J_2[u_2, P_1]$. In contrast to Figure 10 where we only saw $\mathfrak{G}_1$ and $\varphi_{\mathrm{b},1}^2$ here we really would expect to see the influence of all the three terms $-X_3\partial_2\zeta_3^2$, $\mathfrak{G}_2$ and $\varphi_{\mathrm{b},2}^2$ which build up the leading term of the expansion. The reason for this difference is that in the boundary layer zone $\partial_2\zeta_3^2$ coincides with $\partial_n\zeta_3^2$ due to the fact $x_2 \equiv n$ there. In contrast to $\partial_s\zeta_3^2$ in the previous graph, now $\partial_n\zeta_3^2$ is in general non-zero for $x_2 = 0$, compare Theorem 5.1 of [3], so that its Taylor series with respect to x_2 around $x_2 = 0$ starts with the constant term and hence now should be visible in the graph. Indeed this fact can be stated in the figure. In the boundary layer zone we see $J_2[u_2, P_1]$ varying due to the effect of $\varphi_{\mathrm{b},2}^2$. Although $J_2[u_2, P_1]$ becomes more or less constant as we move inside the plate, this constant cannot be only the effect of $\mathfrak{G}_2$, since the value of the constant is approximately -0.0004 and not $-1/90$ as in the previous graph. This discrepancy is in fact produced by the presence of $-X_3\partial_n\zeta_3^2$ in the leading term, or better by the constant term of its Taylor series in x_2 in the same manner as it is explained above.

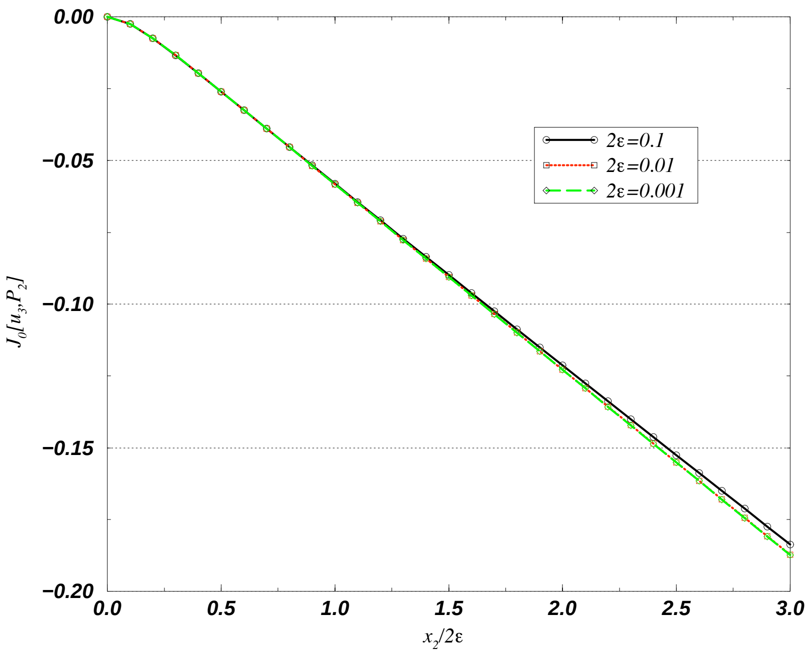

Figure 9: *Hard Clamped* $J_2[u_3, P_0]$.

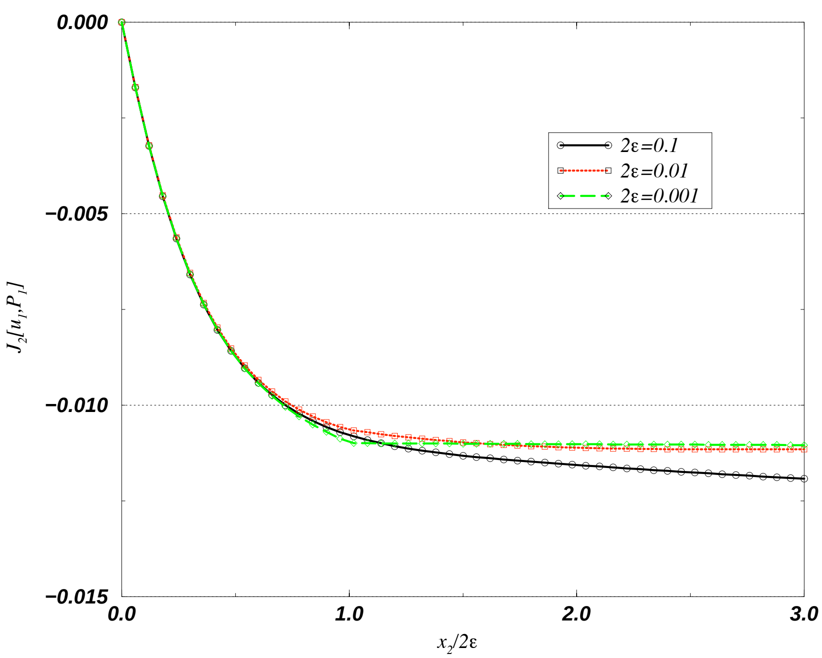

Figure 10: *Hard Clamped* $J_2[u_1, P_1]$.

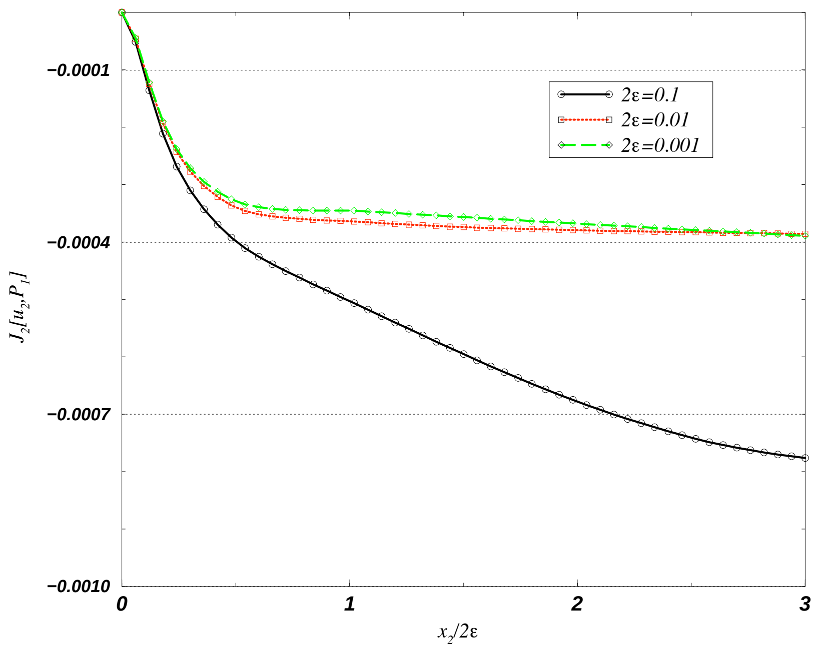

Figure 11: *Hard Clamped* $J_2[u_2, P_1]$.

4.3 Hard clamped plate, membrane response of order 2

The next example is a membrane one with the loadings: $f_\alpha = -1$, $f_3 = 0$, $t_\alpha^\pm = \varepsilon$, $t_3^\pm = 0$, which in accordance with Corollary 3.4 produces an order 2 response.

The values of the considered functionals are for $m = 2$ independent of ε which indicates that the asymptotic expansion starts in accordance with the analysis with ε^2. We first consider the first component of the displacement field u_1. The behavior of the second component is very similar.

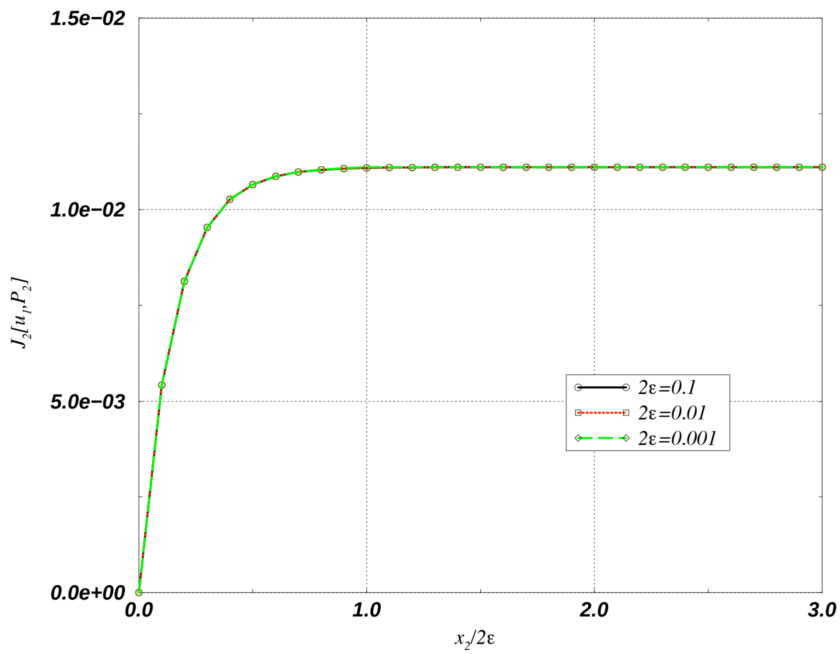

Figure 12: *Hard Clamped* $J_2[u_1, P_2]$.

In Figure 12 we present $J_2[u_1, P_2]$. The graph shows clearly the existence of a boundary layer profile in the leading term of the expansion. This boundary layer profile is only present in a vicinity of the lateral boundary. Since in this case $\mathfrak{G}_1$ is simply a multiple of the Legendre polynomial P_2, compare Corollary 3.4, and ζ_1^2 is of course a constant in X_3, $J_2[u_1, P_2]$ tends to a constant as we move away from the boundary, representing the presence of $\mathfrak{G}_1$.

In Figure 13 $J_2[u_1, P_4]$ shows, as in the preceding graph, a boundary layer behavior in a vicinity of the lateral boundary but then in contrast to it becomes zero outside the boundary layer, since as said above $\mathfrak{G}_1$ is a multiple of P_2 and hence orthogonal to P_4.

In Figure 14 we visualize with the help of $J_2[u_3, P_1]$ the behavior of the third component of the displacement field u_3. We see a boundary layer behavior in a neighborhood of the lateral boundary and then the considered functional tends to zero as we move away from the boundary. The same behavior is visible for $J_2[u_3, P_3]$ (not presented herein).

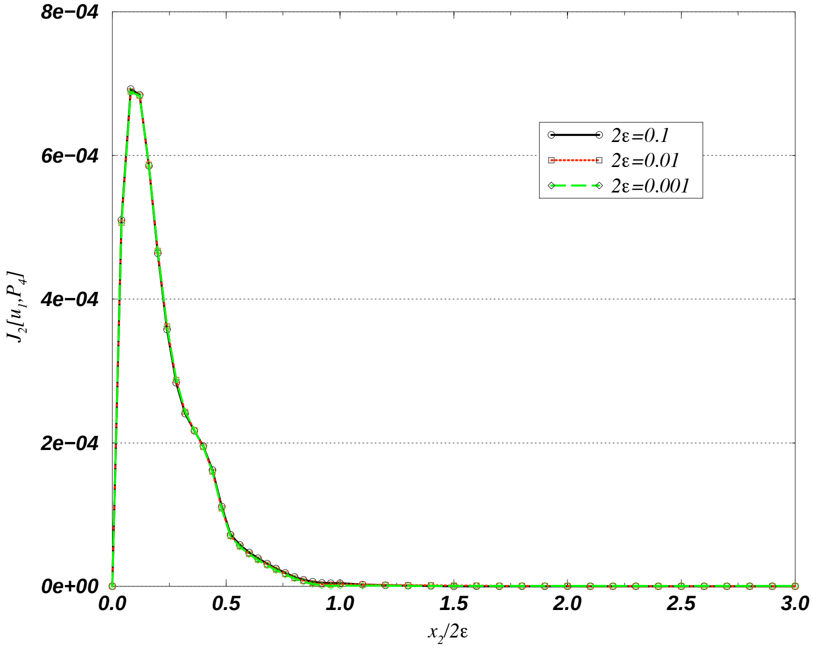

Figure 13: *Hard Clamped* $J_2[u_1, P_4]$.

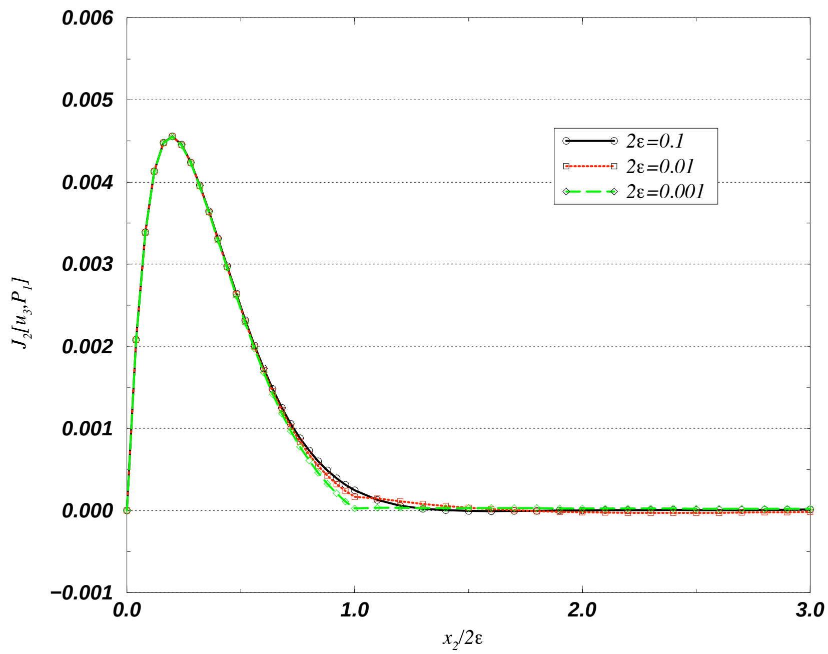

Figure 14: *Hard Clamped* $J_2[u_3, P_1]$.

4.4 Hard clamped vis free lateral boundary conditions

The last example which we investigate shows the influence of the lateral boundary conditions on the higher-order responses. We consider the following bending loadings: $f_\alpha = 0$, $f_3 = \varepsilon(X_3^2 - \frac{1}{3})$, $\boldsymbol{t}^\pm = 0$. In accordance with Corollary 3.6 this loading produces an order 3 response in the hard clamped plate, but according to Theorems 3.9 and 3.10 only an order 2 response in the free plate.

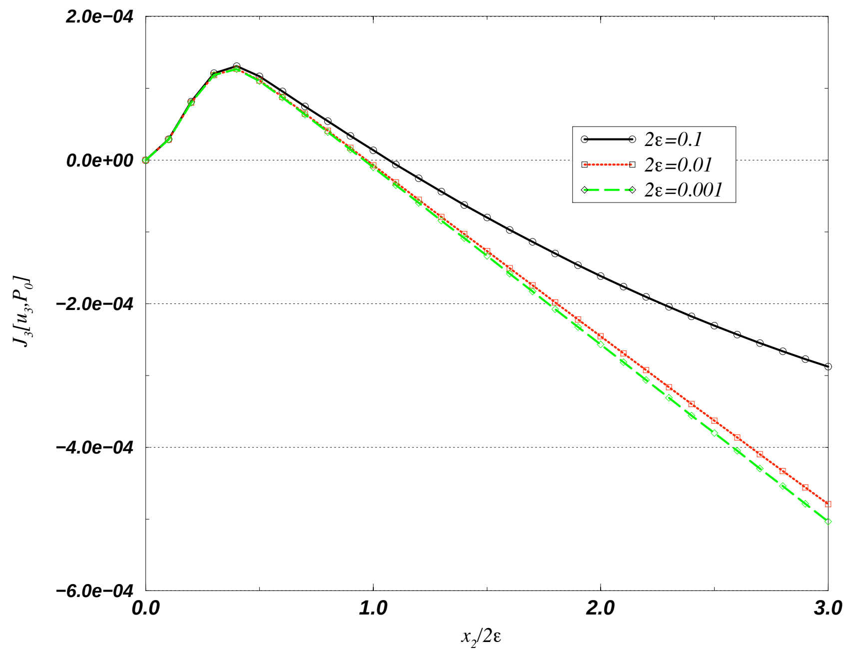

Figure 15: *Hard Clamped* $J_3[u_3, P_0]$.

In Figure 15 one notices the behavior of $J_3[u_3, P_0]$ in the hard clamped case. Convergence for $m = 3$ is noticed (and small values of ε, which is not that fast as $\varepsilon \to 0$) although $m = 2$ would be the correct value predicted by the analysis. But this can be explained analogously to Figure 9 by the Taylor expansion of ζ_3^3 with respect to x_2 around $x_2 = 0$ and the fact that due to the boundary condition $\zeta_3^3 = 0$ on $\partial\omega$, this Taylor series starts with the linear term and hence altogether in x_2/ε with ε^3.

For the free lateral boundary conditions we first consider the behavior of $J_1[u_3, P_0]$ as shown in Figure 16. As predicted by the analysis here $m = 1$ is the right choice. In contrast to the hard clamped situation now the constant part of the Taylor series of ζ_3^2 with respect to x_2 around $x_2 = 0$ is present and non-zero for free lateral boundary conditions. In comparison with the preceding graph now the dramatic influence of the lateral boundary condition on the higher-order response is visible which manifests itself in the discrepancy of the values of m in the considered lateral boundary conditions ($m = 1$ in the free and $m = 3$ in the hard clamped case). We emphasize that although the same loading is

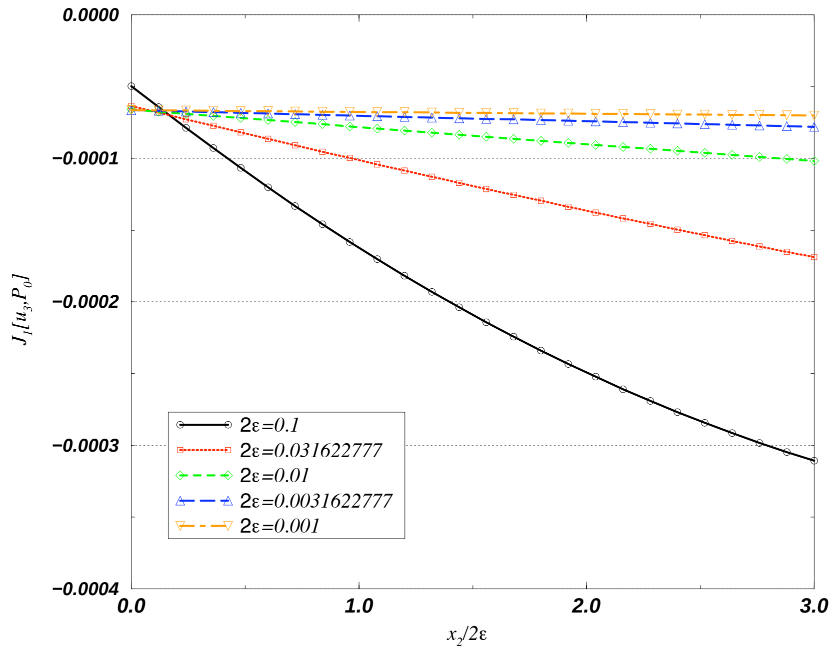

Figure 16: *Free* $J_1[u_3, P_0]$.

considered in both cases of lateral boundary conditions, the asymptotic expansion in the hard clamped case starts with two powers of ε later than in the free one.

Actually the discrepancy of the ε-powers in the asymptotic expansions is indeed only one power of ε, since one more ε-power is due to the different behavior of the Taylor series of the leading generators in the two different cases of boundary conditions. This different behavior is due to the fact that we evaluate the functionals with respect to the scaled variable x_2/ε although in reality the leading generators in the expansion depend on the physical variable x_2. That this is indeed the explanation can be seen easily by first subtracting from $J_1[u_3, P_0]$ its limit value for $x_2 = 0$ and then dividing the result once more by ε, see Figure 17. Then the curves of the corresponding different ε-values do overlap. This action corresponds to a proceeding in which we neglect the constant term in the Taylor expansion of ζ_3^2 with respect to x_2 around $x_2 = 0$, hence starting with the linear term as in the hard clamped situation. Then of course we would have $m = 2$ analogously to the hard clamped case, which reveals that we have indeed only one power of ε deviation in the asymptotic expansions and the other power is due to the evaluation of the functionals with respect to the 'wrong' variable.

The reason for the dramatic change in the asymptotic expansion depending on the lateral boundary conditions is exclusively due to the presence of the Kirchhoff-Love term ζ_3^2 in the free situation. This fact is verified by the two graphs in Figures 18-19, where we show the behavior of the functional $J_3[u_3, P_2]$ for hard clamped and free lateral boundary conditions. Let us recall that the Kirchhoff-Love terms are orthogonal to P_2 and thus are

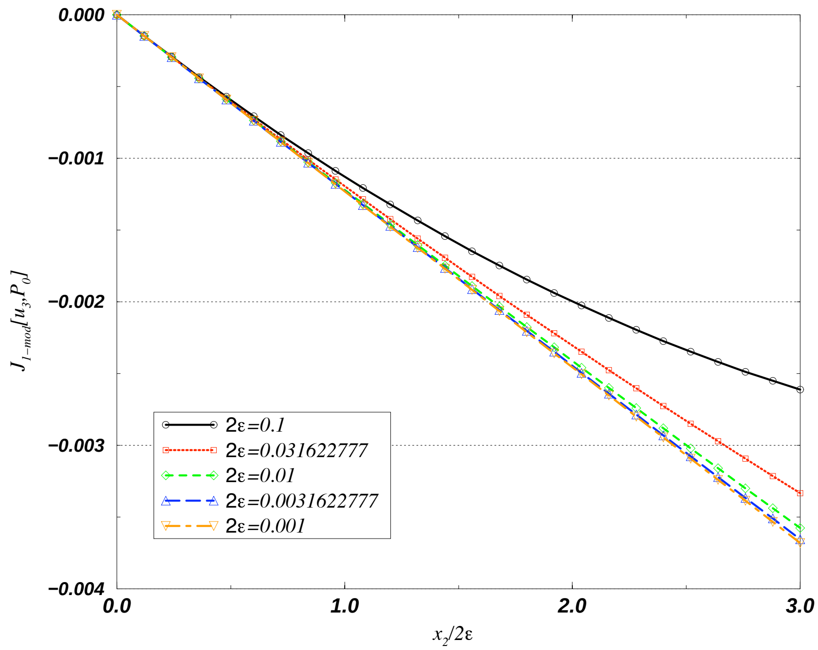

Figure 17: *Free* $[J_1[u_3, P_0] - J_1[u_3, P_0]_{x_2=0}]/(2\varepsilon)$.

invisible in $J_3[u_3, P_2]$. We see that apart from the boundary layer profiles which clearly have to differ from each other, the same behavior independent of the lateral boundary conditions is noticed. In both cases $J_3[u_3, P_2]$ tends to the same constant as we move away from the boundary layer zone which is due to the presence of $\mathfrak{H}_3$.

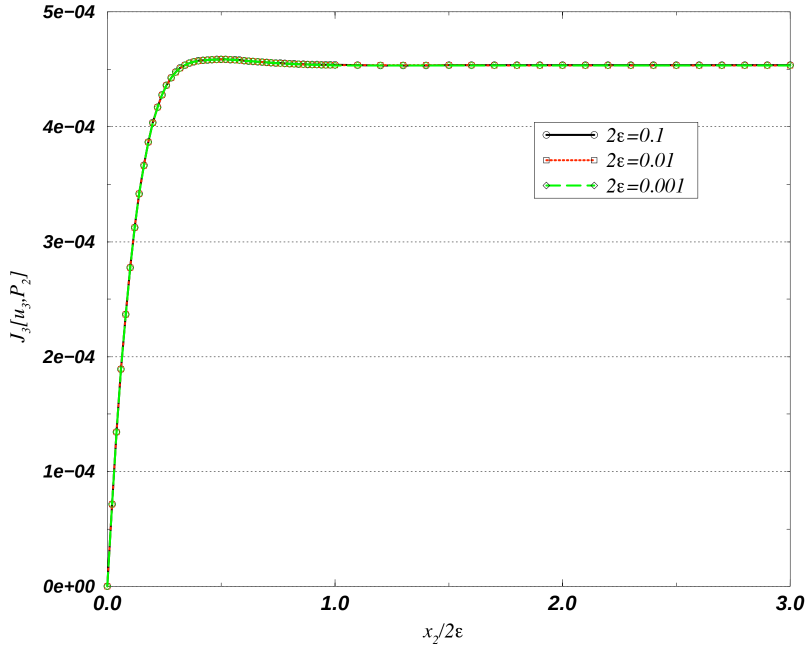

Figure 18: *Hard Clamped* $J_3[u_3, P_2]$.

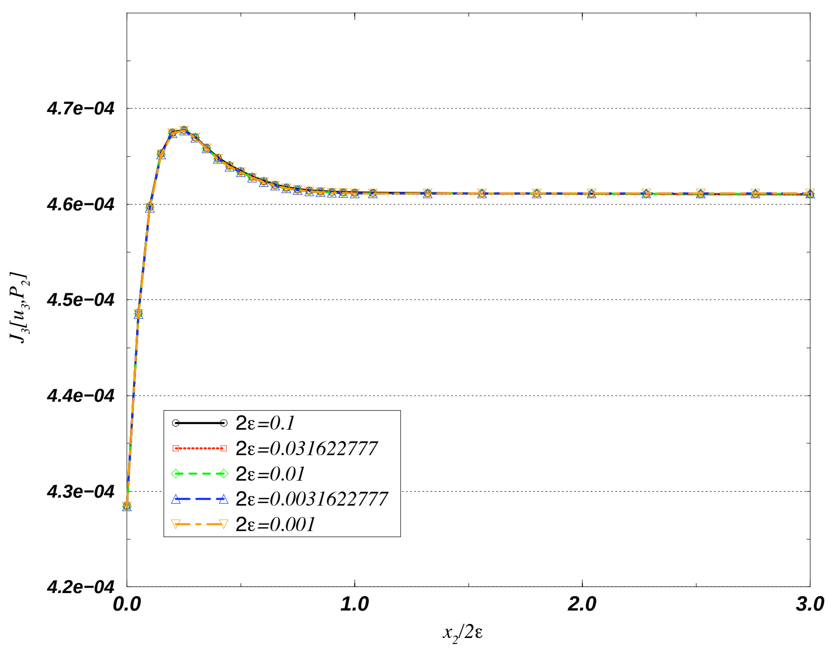

Figure 19: *Free* $J_3[u_3, P_2]$.

5 CONCLUSIONS

If the first moments of the loading are zero, the limit Kirchhoff-Love displacement vanishes. But the three-dimensional displacement is not zero and the knowledge of a number of terms in the asymptotic expansion is necessary if one wants to understand the nature of the response of the thin structure. Contrary to the standard case, the first non-zero term combines in general a Kirchhoff-Love displacement with a boundary layer term and a displacement resulting from higher-order moments of the loading.

We can quantify this fact by an evaluation of the orders of magnitude of the elastic energy $\int_\Omega [A]\boldsymbol{e}(\boldsymbol{u}):\boldsymbol{e}(\boldsymbol{u})$ of the different terms involved in standard and higher-order responses. For a standard response, the energy of the limit Kirchhoff-Love displacement is $\mathcal{O}(\varepsilon)$, like that of the further term $\varepsilon\boldsymbol{v}^1$, compare (2.6), (2.11)-(2.12), and the boundary layer term $\varepsilon\boldsymbol{\varphi}^1$ has a $\mathcal{O}(\varepsilon^2)$ energy. But for a response of order 2, the energy of the Kirchhoff-Love displacement is $\mathcal{O}(\varepsilon^5)$, less than the energy of $\varepsilon^2\mathfrak{G}(\boldsymbol{f},\boldsymbol{t}^\pm)$ which is $\mathcal{O}(\varepsilon^3)$, and still less than the energy of $\varepsilon^2\boldsymbol{\varphi}^2$ which is $\mathcal{O}(\varepsilon^4)$, compare (3.1). The comparison is similar for responses of order 3.

Concerning the loading cases that we numerically investigated, computations were always in accordance with the structure of the first non-zero term in the asymptotics as forecast by the theory. From the practical point of view, it is important to realize that bending loading conditions may exist such that the vertical displacement does not approach infinity as the thickness of the plate tends to zero (Kirchhoff-Love behavior), but may even approach to zero.

Thus, higher-order responses yield less energetic displacements (the energy has the same behavior than in the case when the plate is fixed on one of its faces $\Gamma^\pm$). But the maximum energy is concentrated in a boundary layer term and in displacement resulting from higher-order moments of the loading.

An important question resulting from the presented analysis is associated with dimensionally reduced plate models, i.e., if one of the explicit bending loading conditions would have been applied to a plate model, would it manifest the higher order response as the corresponding 3-D plate? Unfortunately, this question remains open (except for the Kirchhoff-Love model which one knows it cannot mimic the boundary layers zone), because the tractions $\boldsymbol{t}^\pm$ cannot be specified on dimensionally reduced plate models.

ACKNOWLEDGEMENT

The third author expresses his gratitude to profs. W. Wendland and E. Ramm for their invitation to Stuttgart University under Graduiertenkolleg “Modellierung und Diskretisierungsmethoden für Kontinua und Strömungen” where this paper has been initiated.

REFERENCES

[1] P. G. CIARLET. *Mathematical Elasticity. Vol. II, Theory of Plates*. North-Holland, Amsterdam 1997.

[2] M. Dauge, I. Djurdjevic, A. Rössle. Full asymptotic expansions for thin elastic free plates. *C. R. Acad. Sci. Paris, Sér. I,* **326** (1998) 1243–1248.

[3] M. Dauge, I. Djurdjevic, A. Rössle. Higher order bending and membrane responses of thin linearly elastic plates. *C. R. Acad. Sci. Paris, Sér. I,* **326** (1998) 519–524.

[4] M. Dauge, I. Gruais. Asymptotics of arbitrary order for a thin elastic clamped plate. I: Optimal error estimates. *Asymptotic Analysis* **13** (1996) 167–197.

[5] M. Dauge, I. Gruais. Asymptotics of arbitrary order for a thin elastic clamped plate. II: Analysis of the boundary layer terms. *Asymptotic Analysis* **16** (1998) 99–124.

[6] M. Dauge, I. Gruais, A. Rössle. The influence of lateral boundary conditions on the asymptotics in thin elastic plates. To appear in *SIAM Jour. of Math. Anal.* (1999).

[7] M. Dauge, Z. Yosibash. Boundary layer realization in thin elastic 3-d domains and 2-d hierarchic plate models. To appear in *Internat. J. Solids Structures* (1999).

[8] V. G. Maz'ya, S. A. Nazarov, B. A. Plamenevskii. *Asymptotische Theorie elliptischer Randwertaufgaben in singulär gestörten Gebieten I.* Mathematische Monographien, Band 82. Akademie Verlag, Berlin 1991.

[9] V. G. Maz'ya, S. A. Nazarov, B. A. Plamenevskii. *Asymptotische Theorie elliptischer Randwertaufgaben in singulär gestörten Gebieten II.* Mathematische Monographien, Band 83. Akademie Verlag, Berlin 1991.

[10] S. A. Nazarov, I. S. Zorin. Edge effect in the bending of a thin three-dimensional plate. *Prikl. Matem. Mekhan.* **53 (4)** (1989) 642–650. English translation *J. Appl. Maths. Mechs.* (1989) 500–507.

[11] O. A. Oleinik, A. S. Shamaev, G. A. Yosifian. *Mathematical Problems in Elasticity and Homogenization.* Studies in mathematics and its applications. North-Holland, Amsterdam 1992.

[12] A. Rössle. Asymptotische Entwicklungen für dünne Platten im Rahmen der linearen Elastostatik. Doctoral Dissertation, Mathematisches Institut A, Universität Stuttgart, Germany 1999.

[13] B. Szabó, I. Babuška. *Finite Element Analysis.* Willey, New-York 1991.